Monthly Notices
of the
ROYAL ASTRONOMICAL SOCIETY

MNRAS **507,** 5403–5414 (2021)
Advance Access publication 2021 August 24

https://doi.org/10.1093/mnras/stab2408

Physical characterization of equal-mass binary near-Earth asteroid 2017 YE5: a possible dormant Jupiter-family comet

F. Monteiro [1]★ E. Rondón [1] D. Lazzaro [1]★ J. Oey,[2] M. Evangelista-Santana,[1] P. Arcoverde,[1] M. De Cicco [1] J. S. Silva-Cabrera [3] T. Rodrigues[1] and L. B. T. Santos[4]

[1]*Observatório Nacional, R. Gen. José Cristino, 77 - São Cristóvão, 20921-400 Rio de Janeiro, RJ, Brazil*
[2]*Blue Mountains Observatory, 94 Rawson Pde. 2780 Leura, New South Wales 2780, Australia*
[3]*CONACYT – Instituto de Astronomía, Universidad Nacional Autónoma de México (IA-UNAM), AP 106, Ensenada 22800, BC, Mexico*
[4]*Division of Space Mechanics and Control, INPE, C.P. 515, São José dos Campos, 12227-310 São Paulo, SP, Brazil*

Accepted 2021 August 18. Received 2021 August 18; in original form 2021 May 23

ABSTRACT

Photometric observations of the nearly equal-mass binary near-Earth asteroid 2017 YE5 were carried out at the Observatório Astronômico do Sertão de Itaparica (OASI, Brazil) and at the Blue Mountains Observatory (BMO, Australia) between 2018 July and August, shortly after it made a close approach to Earth in 2018 June. These observations allowed to determine an orbital period of the system in good agreement with the result of the radar observations. Our results also indicate that the 2017 YE5 system is not fully locked in a synchronous spin–orbit resonance, as there is a possible asynchronous component or tumbling rotator in the system. Additional data obtained at the Observatorio Astronómico Nacional de San Pedro Mártir (OAN-SPM, Mexico) in 2018 August allowed to derive the colour indices and the low-resolution spectrum, which indicate that the object has a very reddish surface similar to the outer Solar system objetcs. This is consistent with a dark albedo of about 3 per cent, derived from an effective diameter of the combined components and an absolute magnitude of 19.2. Infrared data obtained at the NASA's Infrared Telescope Facility exhibit a thermal emission in the 2.5 μm range for which a low albedo of 2–4 per cent was adjusted by applying a thermal model. Regarding to the taxonomic classification, we found that the 2017 YE5 is a D-type in the Bus-DeMeo taxonomy. Therefore, according to our results and considering that the 2017 YE5 system has a typical comet orbit ($T_J = 2.87$), we suggest that it is a dormant Jupiter-family binary comet.

Key words: techniques: photometric – techniques: spectroscopic – minor planets, asteroids: individual: 2017 YE5.

1 INTRODUCTION

The identification of binary systems among the near-Earth asteroids (NEAs) has grown considerably in recent years, mainly due to detections made by radar observations and to the increase in the number of photometric light curves. It is estimated that about 15 per cent of NEAs larger than 0.2 km are binaries, with the majority being formed by one larger primary component rotating rapidly, and a much smaller secondary component, generally referred to as satellite (Margot et al. 2002; Pravec et al. 2006; Pravec & Harris 2007). One possible explanation for NEA binary formation could be the rotational disruption of reacumulated bodies, likely as a result of the Yarkovsky–O'Keefe–Radzievskii–Paddack (YORP) effect (Pravec & Harris 2007; Walsh, Richardson & Michel 2008; Pravec et al. 2010; Jacobson & Scheeres 2011; Walsh & Jacobson 2015). This effect is the anisotropic thermal re-emission of sunlight by a rotating asteroid, creating torques that modify its rotational period and spin-axis pole (Rubincam 2000; Vokrouhlický, Nesvorný & Bottke 2003; Hanuš et al. 2011, 2013). Thus, the binary formation can occur after the increase in the asteroid rotation rate due to the YORP effect, causing the centrifugal force to overcome the self-gravity of the rubble pile aggregates and the asteroid to shed mass from the equator and subsequently form a secondary component (as modelled by Walsh et al. 2008). Moreover, other binary formation mechanisms are predicted for different populations and size ranges of asteroids, such as capture, collisions, and tidal processes (Merline et al. 2002; Margot et al. 2015; Walsh & Jacobson 2015). Therefore, to achieve a better understanding of the formation and evolution of these systems is necessary to known their physical properties.

NEA 2017 YE5 made an Earth close approach on 2018 June 21 at a distance of about 0.04 au. This object has a semimajor axis (a) of 2.82 au, an eccentricity (e) of 0.71, and an inclination (i) of 6.22 deg. It is also classified as a Potentially Hazardous Asteroid (PHA) by JPL's Small-Body Database Browser, as it has a minimum orbital intersection distance (MOID) with respect to the Earth less than 0.05 au and an absolute magnitude $H \leq 22$. During its close Earth flyby it became an interesting radar target for Arecibo, Goldstone, and Green Bank Observatories. Thus, radar observations performed between 2018 June 21 and 26 from these radio telescopes showed that 2017 YE5 is actually composed of two asteroids of similar size and mass in mutual orbit about each other (Taylor et al. 2018, 2019). To date, only four near equal-mass binaries have been discovered among the NEA population, including (69230) Hermes, (190166) 2005 UP156, 1994 CJ1, and 2017 YE5.

★ E-mail: filipeastro@on.br (FM); lazzaro@on.br (DL)

The radar observations indicated that both components in the 2017 YE5 system have about 900 m in diameter, slight different spherical shapes and possibly different radar scattering properties (Taylor et al. 2018, 2019). Close flyby of 2017 YE5 also provided an excellent opportunity for systematic photometric observations using small ground-based telescopes (e.g. Warner 2018). This is very interesting because the radar and optical observations are very complementary and can allow to constrain their physical properties, including their masses and densities (Scheirich & Pravec 2009; Margot et al. 2015). For this reason, in general, binary asteroids are interesting targets for studies on internal structure and composition.

The Tisserand parameter (T_J) is often employed to distinguish between asteroid and comet orbits with reference to the Sun and Jupiter as the major influencing bodies. For the 2017 YE5 system, this parameter is $T_J = 2.87$, implying a typical Jupiter-family comet orbit, as defined by Levison & Duncan (1994) ($2 < T_J < 3$). In addition, it has a MOID with respect to Jupiter of 0.42 au and it is quite close to the 5:2 mean motion resonance with Jupiter, whose center is located at $a = 2.825$ au. All these facts led us to investigate the nature of this binary asteroid using data from different observatories. Thus, we carried out photometric follow-up of the 2017 YE5 system during its close flyby to determine its physical properties. In this work, we present results from our full characterization of 2017 YE5 using photometric and near-infrared spectroscopy data to constrain its orbital and rotational period, colour indices, albedo, taxonomic type and probable source region. Finally, we compare our results with those previously reported from radar observations.

2 PHOTOMETRIC STUDY

2.1 Observations and data reduction

Photometric observations of 2017 YE5 system were made at the Observatório Astronômico do Sertão de Itaparica (MPC code Y28, OASI - Nova Itacuruba) on six nights in 2018 July, within the framework of the IMPACTON project. The images were acquired with the 1.0 m *f*/8 Classic Cassegrain Telescope and an Apogee Alta U42 CCD camera with a 2048 × 2048 array of 13.5 μm pixels in a 2 × 2 binning mode. This configuration provides a field in the focal plane of 11.8 × 11.8 arcmin and has an image scale of 0.343 arcsec per pixel (unbinned). Additional information on the OASI can be found in Rondón et al. (2020). The exposure time of the observations was adjusted according to the asteroid's brightness and sky motion. The light-curve observations were performed using the sidereal tracking and an R-Johnson-Cousins filter.

Photometric light-curve observations were also made from Blue Mountains Observatory (MPC code Q68 - BMO, Australia) where three telescopes system were used to observe the 2017 YE5 system. These observations occurred between 2018 July and August, using four different CCD cameras. Table 1 shows the observing circumstances and instruments used for all observations. The physical characteristics of the instruments used in the BMO are given in Table 2. The telescopes were set in sidereal tracking and the object was observed over several nights for 2–7 h. Images taken with all telescopes were unfiltered with exposures ranging from 60 to 180 s (with the exception of one night) to prevent trails due to the fast-apparent motion of the asteroid during its close approach.

The science images acquired to generate light curves were calibrated using the Maxim DL software following the standard procedures of data reduction, i.e. master-dark subtraction and master-flat correction. The flat-field frames and the dark frames were taken at the beginning and the end of each observation night, respectively. All data measurements for light curves were made using MPO Canopus V10. In the case of BMO data, instrumental magnitudes were converted to V-Johnson-Cousins magnitudes using solar-coloured field stars from a version of the CMC-15 catalogue (http://svo2.cab.inta-csic.es/vocats/cmc15/) distributed with MPO Canopus. The OASI data set was maintained in *R* band. To generate the light curves, we obtained the reduced magnitude, i.e. the corrected magnitude to a unity distance by applying -5 log(rΔ) to the observed magnitudes with r and Δ being, respectively, the asteroid's distances from the Sun and from the Earth in au.

To obtain a photometric spectrum, an additional observation from the OASI was made using the *g*−*r*–*i*–*z* *Sloan Digital Sky Survey* (*SDSS*) filters. This observation occurred on 2018 August 9 and was performed by alternating each filter in the system, repeating four times in order to obtain an averaged spectrum. The images were obtained using the differential tracking mode to avoid trails due to the long exposure times (see Table 1). Additionally, using the Observatorio Astronómico Nacional de San Pedro Mártir (code 679, OAN-SPM), we observed 2017 YE5 system using photometry with four different broad-band filters (*BVRI* Johnson–Cousins filters) to obtain another photometric spectrum. This observation was made with a 2.1 m *f*/7.5 telescope and FLI E2V-4240 CCD camera of 2048 × 2048 array of 13.5 μm pixels in a 2 × 2 binning mode. This configuration gives a field of view of approximately 11.8 × 11.8 arcmin and an image scale of 0.176 arcsec pix^{-1}. This observation occurred on 2018 August 18 when the apparent magnitude of the asteroid was of about 20.

The data reduction in the both cases described above was performed using the Image Reduction and Analysis Facility (IRAF) software, also following the standard procedures. In order to determine the extinction coefficient and the zero-point of the night, selected standard stars (from Landolt 1992; Smith et al. 2002) were observed at different air masses over the night and in the same filters. The instrumental magnitudes of 2017 YE5 and of the standard stars were measured using aperture photometry with the task PHOT of the IRAF. The zero-point of the night is calculated from the difference between the catalogue magnitude of the standard star and the above-atmosphere instrumental magnitude of the standard star. The latter being the magnitude corrected for the atmospheric extinction. Lastly, the zero-point is removed from the above-atmosphere instrumental magnitude of the asteroid to find its calibrated magnitude. It is noteworthy that when the standard star was not observed at various air masses, we used several calibrated field stars to compute the zero-point of the night.

2.2 Light-curves analysis

One of the physical properties of the asteroids that can be directly derived from Earth observations is the rotational period, which is determined by analysis of lightc urves obtained through photometric data. The light curves also hold clues about the shapes and the surface variegation of asteroids, as well as they can reveal features that are common among binary asteroids. The most widely used period analysis method is the Fourier series analysis developed by Harris et al. (1989). This method easily provides us the rotational period of asteroids from fragmented light-curves data.

In the case of binary asteroids, the complex light curves require more attention, because each of the two components scatters sunlight and produces its own rotational light curve. In addition, brightness attenuation produced by mutual events (eclipses/ocultations) can be observed in the combined light curves of the system's components, whenever the geometric configuration of the observations

Table 1. Observational circumstances of the 2017 YE5 system. For each date, the table shows the telescopes, filters, and cameras used, the apparent magnitude (V) and the exposure time, as well as the asteroid's distance from Earth (Δ) and from the Sun (r), and the solar phase angle (α), at the middle point of the observation interval.

Date	Telescope	Filter	Camera	Exposure time	V	r (au)	Δ (au)	α (°)
Blue Mountains Observatory – BMO								
2018/07/05	0.35 m *f*/7 SCT Edge	Clear	SBIG ST8300	180	16.07	1.1363	0.1293	21.09
2018/07/06	0.61 m *f*/6.8 CDK	Clear	Apogee U6M	60	16.17	1.1460	0.1381	19.27
2018/07/06	0.61 m *f*/6.8 CDK	Clear	Apogee U6M	60	16.19	1.1477	0.1396	18.97
2018/07/13	0.61 m *f*/6.8 CDK	Clear	Apogee U6M	120	16.8	1.2162	0.2032	9.32
2018/07/15	0.61 m *f*/6.8 CDK	Clear	Apogee U16M	120	16.96	1.2372	0.2233	7.83
2018/07/16	0.61 m *f*/6.8 CDK	Clear	Apogee U16M	120	17.04	1.2471	0.2328	7.11
2018/07/17	0.61 m *f*/6.8 CDK	Clear	Apogee U16M	120	17.11	1.2559	0.2415	6.58
2018/07/18	0.61 m *f*/6.8 CDK	Clear	Apogee U16M	120	17.19	1.2660	0.2514	6.1
2018/07/19	0.61 m *f*/6.8 CDK	Clear	Apogee U16M	120	17.28	1.2768	0.2622	5.76
2018/07/20	0.61 m *f*/6.8 CDK	Clear	Apogee U16M	120	17.38	1.2869	0.2724	5.6
2018/07/21	0.61 m *f*/6.8 CDK	Clear	Apogee U16M	120	17.47	1.2971	0.2828	5.61
2018/07/22	0.35 m *f*/5.9 SCT	Clear	SBIG ST8XME	180	17.57	1.3069	0.2928	5.76
2018/07/22	0.61 m *f*/6.8 CDK	Clear	Apogee U16M	180	17.58	1.3072	0.2931	5.76
2018/07/22	0.35 m *f*/7 SCT Edge	Clear	SBIG ST8300	180	17.59	1.3082	0.2942	5.79
2018/07/24	0.61 m *f*/6.8 CDK	Clear	Apogee U16M	180	17.81	1.3290	0.3158	6.46
2018/07/24	0.35 m *f*5.9 SCT	Clear	SBIG ST8XME	300	17.82	1.3300	0.3169	6.5
2018/07/25	0.35 m *f*/5.9 SCT	Clear	SBIG ST8XME	300	17.92	1.3395	0.3270	6.92
2018/07/25	0.35 m *f*/7 SCT Edge	Clear	SBIG ST8300	180	17.93	1.3400	0.3275	6.94
2018/07/31	0.35 m *f*/5.9 SCT	Clear	SBIG ST8XME	180	18.56	1.4003	0.3937	10.13
2018/08/10	0.35 m *f*/5.9 SCT	Clear	SBIG ST8XME	180	18.65	1.4098	0.4046	10.65
2018/08/04	0.35 m *f*/5.9 SCT	Clear	SBIG ST8XME	300	18.95	1.4404	0.4402	12.29
2028/08/04	0.35 m *f*/7 SCT Edge	Clear	SBIG ST8300	180	18.96	1.4418	0.4419	12.37
2018/08/05	0.35 m *f*/7 SCT Edge	Clear	SBIG ST8301	180	19.05	1.4514	0.4535	12.87
Observatório Astronômico do Sertão de Itaparica - OASI								
2018/07/12	1.0 m *f*/8 CCT	R	Apogee U42	70	16.7	1.2010	0.1890	11.4
2018/07/13	1.0 m *f*/8 CCT	R	Apogee U42	70	16.8	1.2110	0.1982	10.2
2018/07/14	1.0 m *f*/8 CCT	R	Apogee U42	70	16.9	1.2211	0.2078	9.2
2018/07/15	1.0 m *f*/8 CCT	R	Apogee U42	60	17.0	1.2313	0.2175	8.3
2018/07/16	1.0 m *f*/8 CCT	R	Apogee U42	60	17.1	1.2414	0.2273	7.5
2018/07/17	1.0 m *f*/8 CCT	R	Apogee U42	60	17.1	1.2518	0.2374	6.8
2018/08/09	1.0 m *f*/8 CCT	g,r,i,z	Apogee U42	240	19.4	1.4886	0.4989	14.7
Observatorio Astronómico Nacional de San Pedro Mártir - OAN-SPM								
2018/08/18	2.1 m *f*/7.5 RCT	B,V,R,I	FLI E2V-4240	300, 400	20.2	1.5826	0.6231	18.7

Note: SCT is the short for Schimdt Cassegrain Telescope; CDK is the short for Corrected Dahl Kirkham; CCT is the short for Classic Cassegrain Telescope; RCT is the short for Ritchey–Chrétien Telescope.

Table 2. Physical characteristics of the different instruments used to obtain photometric data.

Camera	Array	Pixel size (μm)	Telescope	Diameter (m)	Focal distance (mm)	Design
SBIG ST8300	3326 × 2504	5.4	Edge Celestron	0.35	2450	Schimdt Cassegrain Telescope
SBIG ST8XME	1530 × 1020	9	Classic Celestron	0.35	2106	Schimdt Cassegrain Telescope
Apogee U16M	4096 × 4096	9	Planewave 24	0.61	3980	Corrected Dahl Kirkham
Apogee U6M	1024 × 1024	24	Planewave 24	0.61	3980	Corrected Dahl Kirkham
Apogee U42	2048 × 2028	13.5	Astro Optik	1.0	7030	Classic Cassegrain Telescope
FLI E2V-4240	2048 × 2028	13.5	UNAM	2.12	15 900	Ritchey–Chrétien Telescope

is favourable. Thus, photometric observations of such systems can reveal a signal with two (or more) different periods into a combined light curve. This can be represented as a linear addition of two Fourier series, as initially proposed by Pravec et al. (2006) in the following general form:

$$F(t) = F_1(t) + F_2(t) \quad (1)$$

$$F_1(t) = C_1 + \sum_{k=1}^{m_1}[S_{1k}\sin\frac{2\pi k}{P_1}(t-t_0) + C_{1k}\cos\frac{2\pi k}{P_1}(t-t_0)] \quad (2)$$

$$F_2(t) = C_2 + \sum_{k=1}^{m_2}[S_{2k}\sin\frac{2\pi k}{P_2}(t-t_0) + C_{2k}\cos\frac{2\pi k}{P_2}(t-t_0)], \quad (3)$$

where $F(t)$ is the total reduced flux at time t, t_0 is a zero-point time, $F_j(t)$ are the reduced fluxes of the components at time t, C_j are mean reduced fluxes of the components, C_{jk} and S_{jk} are the Fourier coefficients, P_j are the rotational periods, and m_j are the highest significant order. It is worth mentioning that for the use this method it was assumed that the rotation for each component is around its principal inertia axis. A complex light curve can also be produced by a single asteroid in a state of non-principal axis rotation (Pravec et al. 2005).

Initially, the rotational period was determined using the MPO Canopus, which incorporates the Fourier analysis algorithm (FALC) developed by Alan Harris. As a first hypothesis, it was considered that both components rotate synchronously with their mutual orbital period, as a doubly synchronous binary (e.g. NEA 69230 Hermes).

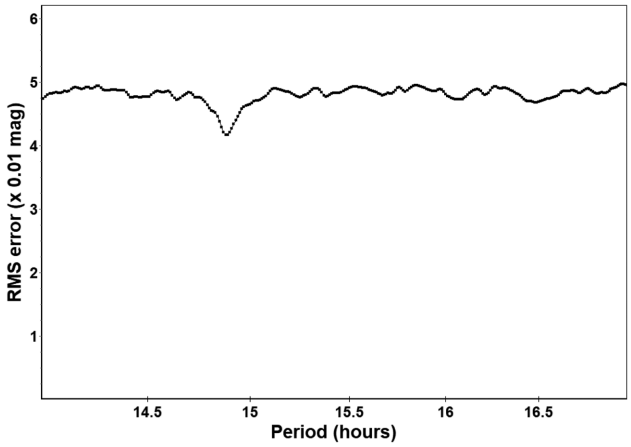

Figure 1. Period spectrum for the light-curve analysis of the 2017 YE5 system. The minimum at 14.88 h represents the rotational period of the primary component of 2017 YE5.

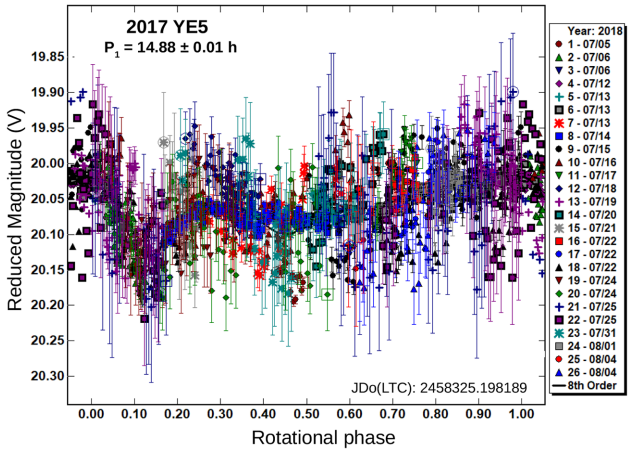

Figure 2. Rotational light curve of an asynchronous component in the 2017 YE5 system. The light-curve fits a period of $P = 14.88$ h.

Thus, applying a simple Fourier series analysis, we found a short primary period, indicated in the period spectrum shown in Fig. 1. In the figure is given the range of periods in the search along the *x*-axis while the RMS error values of the Fourier analysis are displayed along the *y*-axis. In general, the results found with the lowest RMS error corresponds very closely to the actual period. It is noteworthy that we performed the analysis using all light curves from BMO and only three from OASI, since the images obtained on July 15th, 16th, and 17th were rejected because the magnitudes of the asteroid were affected by the brightness of the field stars.

The best-fitting primary period displayed in the period spectrum is $P_1 = 14.88$ h. Its corresponding composite light curve is shown in Fig. 2. In the *x*-axis is given the rotational phase, ranging from −0.05 to 1.05, and in the *y*-axis the reduced magnitude. The different symbols and colours indicate different nights of observation while the continuum line corresponds to the best fit. This result gives a value much shorter than the orbital period of about one day indicated by radar observations. Therefore, the primary period of 14.88 h is likely the rotational period of one of the components of 2017 YE5. This indicate that 2017 YE5 system may not be fully synchronized. Furthermore, the rotational light curve has a small amplitude of about 0.1 mag, indicating an approximately spherical shape for one of the components, which is consistent with the radar images (Taylor et al. 2019).

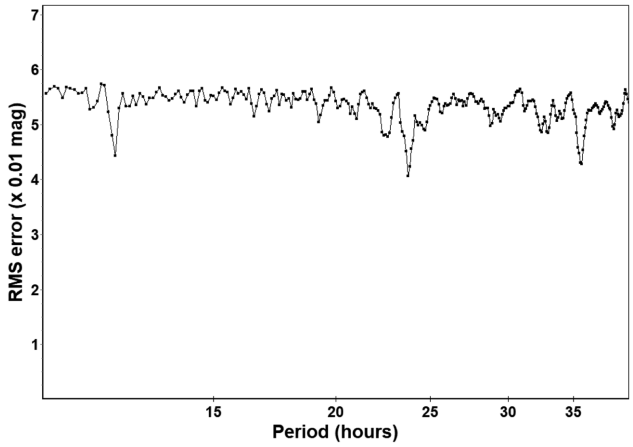

Figure 3. Period spectrum for the light-curve analysis of the 2017 YE5 system. The most likely solutions for the orbital period of the system are 11.9, 23.7, and 35.5 h, which represent the lowest RMS values in the period spectrum.

With this in mind, we carried out a search for the orbital period of the 2017 YE5 system. For this, we used the 'Dual Period Search' tool in Canopus, an algorithm based on the work of Pravec et al. (2006). In the dual-period search initial process, the primary period is derived from the composite light curve, which is subtracted from the original data, leaving only the variations due to the secondary component and mutual events. Thus, the Fourier coefficients of the rotational light curve of $P_1 = 14.88$ h were used to subtract the primary curve from the data, leading to a first approximate orbital period ($P_{\rm orb}$) of about 24 h. Once this is found, the orbital period is subtracted from the data, which allows finding a refined primary period. Then, we repeated these procedures iteratively until the results of the rotational and orbital periods stabilized. From this analysis using two fourier series, we found a satisfactory fit for P_1 and $P_{\rm orb}$. In Fig. 3 is shown the period spectrum of the last iteration for the orbital period, which displays three preferred secondary periods.

Looking at the period spectrum, it is possible to note three minima at about 11.9, 23.7, and 35.5 h, with a stronger signal for the middle one. The first and third are likely rotational aliases, which are usually caused by an miscount of the number of rotations over the time-span of the data. The shortest, for example, appears to be half of the orbital period. Therefore, we considered that the best-fitting solution of 23.706 h represents the orbital period ($P_{\rm orb}$) of the components around their center of mass. The secondary light curve is shown in Fig. 4. This result is in good agreement with the previously results reported by radar observations, which provided an orbital period of roughly 24 h (Taylor et al. 2018, 2019). Another result was reported by Warner (2018), who found a period of 20.6 h from light curves obtained in 2018 June.

Despite their scatter, the orbital light-curve displays mutual events observed on at least four different nights at the BMO. These events appear to be partial, because the first minimum, for example, has a very low attenuation for a system of two components with nearly equal size. It is important to mention that the 2017 YE5 was initially observed very close to the mutual orbit pole in 2018 June by radar telescopes (Taylor et al. 2019). Because of this, the light curves presented in Warner (2018) do not show evidence of mutual events. Then, it is possible that we have observed the 2017 YE5 system in a geometric configuration still far from that which could exhibit

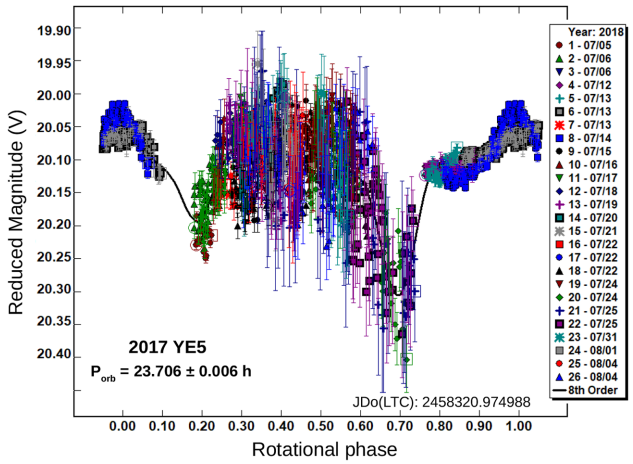

Figure 4. Composite light curve of 2017 YE5 system showing the mutual events. The light-curve fits an orbital period of about 23.7 h. The primary light curve component was subtracted.

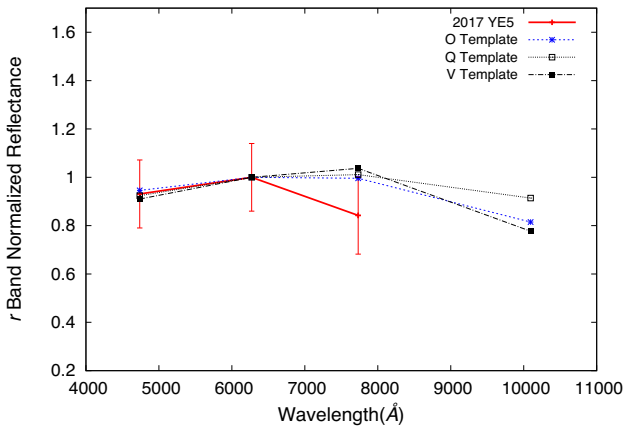

Figure 5. Normalized photometric spectrum of 2017 YE5 obtained using OASI data in the *SDSS* system. The points indicate the normalized reflectance and respective error calculated for each *SDSS* filter. The red solid line represents the observed spectrum while the segmented ones represent templates of three taxonomic types given in Carvano et al. (2010).

total mutual events, with deeper attenuations. In addition, the light curves of binary asteroids can indicate whether the components are orbiting each other in a circular or elliptic orbit. In this case, the light curve of 23.7 h has symmetrically spaced mutual events of 0.5 in the rotational phase, indicating that the components are orbiting each other in a circular orbit.

We also searched for a third additive light curve, which could be related to the rotational period of the second component, presuming that it is not tidally locked, with a rotational period equal to the orbital period. To do this, we did another dual period search, but this time subtracting both the rotational and orbital light curves from the data in search of a third period in the system. However, we did not find a reasonable light curve, suggesting that the second component of the system rotates synchronously with its mutual orbital. On the other hand, it is also possible that the variations due to the rotation of the second component have been lost in the noise of the data.

Knowing that binary asteroids provide a unique opportunity to derive the mean density of the components, we used the determined physical characteristics of the 2017 YE5 system to derive its density. Radar estimates indicate that both components in the 2017 YE5 system are approximately 900 m in diameter and have an orbital separation of 1.8 km (four component radii) (Taylor et al. 2018, 2019). Here, we considered that the actual separation can be up to five component radii, since the two components may not be at their extreme elongation as they would be before/after maximum with a period of about 24 h, then the density would be from 0.6 to 1.2 g cm^{-3} as indicated by applying the third Kepler's law. The latter being a more believable value consistent with various other binaries given in the literature (e.g. Margot et al. 2015).

2.3 Photometric spectrum

The photometric spectrum of an asteroid show how the reflectance of the asteroid's surface varies with the wavelength and, depending of its behaviour, it is classified into a taxonomic class. Thus, the reflectance spectrum provides clues about asteroid surface physical properties and compositions. To derive the photometric spectrum we carried out the same procedure followed by Rondón et al. (2019). For OASI images, in the *SDSS* filters, we transformed the asteroid colour indices $(m_g - m_r)_A$, $(m_i - m_r)_A$, and $(m_z - m_r)_A$ to normalized reflectance at the r filter by removing the solar colours $(m_g - m_r)_\odot$, $(m_i - m_r)_\odot$, $(m_z - m_r)_\odot$,[1] and we rescaled the g, i, and z reflectance using the equation (4). For the OAN-SPM images, we normalized the obtained colour indices $(m_B - m_V)_A$, $(m_R - m_V)_A$, and $(m_I - m_V)_A$ to unity the reflectance at the V filter, and we rescaled the B, R, and I reflectance using the equation (4) modified for the Johnson–Cousins system. In this case, the solar colours removed were extracted of Ramírez et al. (2012)

$$\mathcal{R}_\lambda = 10^{-0.4[(M_\lambda - M_r)_A - (M_\lambda - M_r)_\odot]}. \quad (4)$$

Subsequently, we compared the obtained photometric spectrum with several templates of the taxonomic scheme of Carvano et al. (2010), using a chi-square test to classify our spectra, as used in Rondón et al. (2019). In the case of the OASI spectrum, the comparison with the templates is direct. But, for the OAN-SPM spectrum, we had to first tranform the templates of Carvano et al. (2010) from *SDSS* filters to Johnson–Cousins filters, using the transformation equations given in Jester et al. (2005).

In this way, using the previous procedure with the data acquired at OASI and OAN-SPM on 2018 August 9 and 18, respectively, we obtained the photometric spectra of 2017 YE5 (Figs 5 and 6). By applying the chi-square test with several templates of Carvano et al. (2010) to the spectrum obtained at OASI (Fig. 5) we found that the best fit correspond to Q-type, while the spectrum obtained at OAN-SPM correspond to a D-type (Fig. 6). It is noteworthy that in the OASI spectrum no data is avalilable in the z filter, since the exposure time used to take images in this filter did not produce a good signal-to-noise ratio. Indeed, this lack introduces a large uncertainty in the classification of the OASI spectrum. However, it is known that changes in the reflectance spectrum can be caused by variations on surface composition (e.g. Murchie & Pieters 1996; Mothé-Diniz et al. 2000; Lazzaro et al. 2013), surface roughness (Hapke 1981, 1984), space weathering (e.g. Hapke 2001; Strazzulla et al. 2005; Pieters & Noble 2016), different phase angles and reddening effect (e.g. Reddy et al. 2012; Sanchez et al. 2012; Carvano & Davalos 2015), different shape (e.g. Carvano & Davalos 2015), and presence of coma (e.g. Rondón-Briceño, Carvano & Lorenz-Martins 2017).

Our photometric spectra were obtained at close phase angles, indicating that the difference between them is not associated with

[1] http://www.sdss.org/dr12/algorithms/ugrizvegasun/

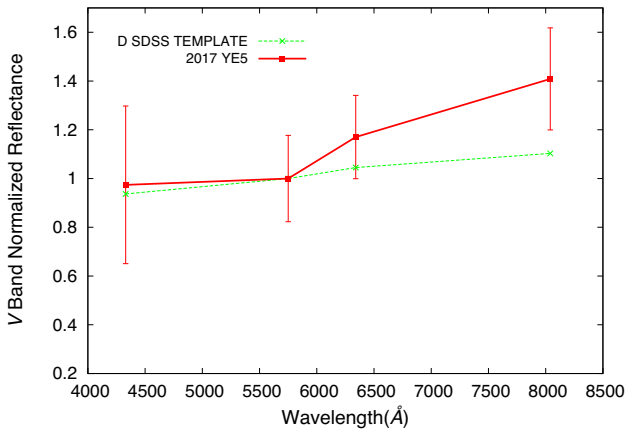

Figure 6. Normalized photometric spectrum of 2017 YE5 obtained using OAN-SPM data in the Johnson–Cousins system. The points indicate the normalized reflectance and respective error calculated for each Johnson–Cousins filter. The red solid line represents the observed spectrum while the segmented one is the template of D-type given in Carvano et al. (2010).

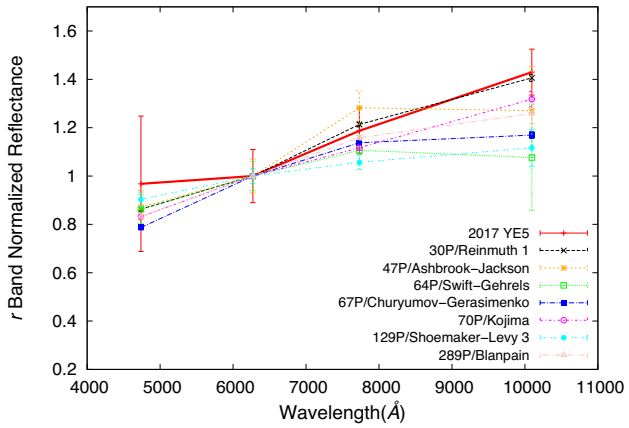

Figure 7. Normalized photometric spectrum of 2017 YE5 compared to different Jupiter-family comets in the *SDSS* system. The colour indices used to derive the reflectances of the comets were obtained in Solontoi et al. (2012).

change in phase angle. On the other hand, radar observations showed that this object is composed of two components with nearly equal size and shape, which exhibit different scattering radar properties (Taylor et al. 2018, 2019). Thus, the difference between our spectra may be due to the components having different compositions or the presence of a coma in one of them. The first hypothesis is plausible since the radar observations identified that the components of 2017 YE5 appear to show a distinct difference in their surface brightness and radar reflectivity, and the second is also plausible since our spectrum in Johnson–Cousins system is a D-type with a very strong red spectral slope, similar to obtained for some Jupiter-family comets (JFC; Fig. 7). This fact is also appreciable in the colour–colour diagram (Fig. 8), where again 2017 YE5 is seen as very reddish, falling among very low albedos objects, such as D-type asteroids and JFCs. This is in good agreement with an albedo of about 3 per cent, derived from the effective system diameter obtained from radar observations and an absolute magnitude of 19.2. It is important to reiterate that the 2017 YE5 system has a typical Jupiter-family comet orbit, with T_J = 2.87, implying in a dormant comet candidate due to its reddish surface. This classification is based on previous works (Fernández, Jewitt & Sheppard 2005; DeMeo & Binzel 2008; Kim, Ishiguro & Usui 2014; Mommert et al. 2015) that identified comet candidates among asteroid-like NEAs using three criteria: $T_J \leq 3$, taxonomy (C, P, T, or D-types in Tholen classification), and/or low (<0.075) albedos. Next section, we will constrain the albedo through flux measurements at near-infrared (0.8–2.5 μm) wavelengths.

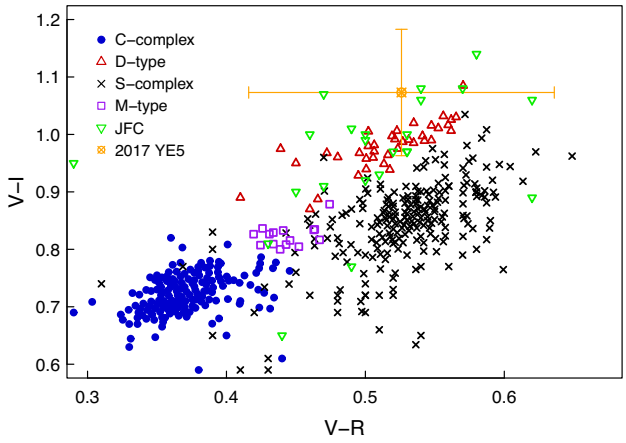

Figure 8. V–*R* versus V-I colour diagram for a sample with different taxonomic types, with 2017 YE5 falling among D-type asteroids and Jupiter-family comets (JFC). The asteroid data are taken from Zellner, Tholen & Tedesco 1985; Ieva et al. 2018, and the JFC data from Lamy & Toth 2009.

In addition, we computed the spectral slope of the D-type spectrum of 2017 YE5 following the S' definition in Luu & Jewitt (1996). We used the wavelength range 0.55 to 0.8 μm (corresponding to the V- and I-band center wavelengths in the Johnson-Cousins system) to measure the spectral slope in units of per cent/1000 Å. Thus, the spectral slope of 2017 YE5 is S' = 15 ± 5 per cent/1000 Å. This value is very compatible with the mean slope of asteroids in cometary orbits (ACOs) (S' = 9.7 ± 4.6 per cent/1000 Å) and with the mean S' of the Damocloids (S' = 12.2 ± 2.4 per cent/1000 Å) presented in Licandro et al. (2018). According to Licandro et al. (2018), objects with $T_J \leq 3$ and S' ≤ 3 per cent/1000 Å are likely C- or B-type interloper asteroids, while objects in cometary orbits with S' > 10 per cent/1000 Å are likely dormant comets.

3 SPECTROSCOPIC STUDY

3.1 Observations and data reduction

Near-infrared (IR) spectroscopic observations (0.8−2.5 μm) of 2017 YE5 were performed using the 3-m NASA's Infrared Telescope Facility (IRTF) at Mauna Kea observatory (Hawaii) on 2018 June 23, within the framework of the MIT−Hawaii Near-Earth Object Survey (MITHNEOS). The near-IR spectrum of 2017 YE5 was obtained using the SpeX infrared spectrometer in prism mode (Rayner et al. 2003) on 2018 June 23 between 12:23 and 13:00 UTC when the apparent magnitude of the asteroid was 15.2 and at a phase angle of 79 deg. Weather conditions were photometric during the observation with an average atmospheric seeing of ∼0.9 arcsec and a relative humidity of ∼13 per cent. Apart from the asteroid, standard stars of solar type were observed to allow removal of the solar spectrum.

Reduction was carried out by the MITHNEOS team using the Image Reduction and Analysis Facility (IRAF) and Interactive Data Language (IDL). The object and standard stars spectra were then run through an IDL code to remove residual atmospheric effects, and finally the corrected object spectrum was divided by the average of the corrected standard star spectra to create the final reflectance

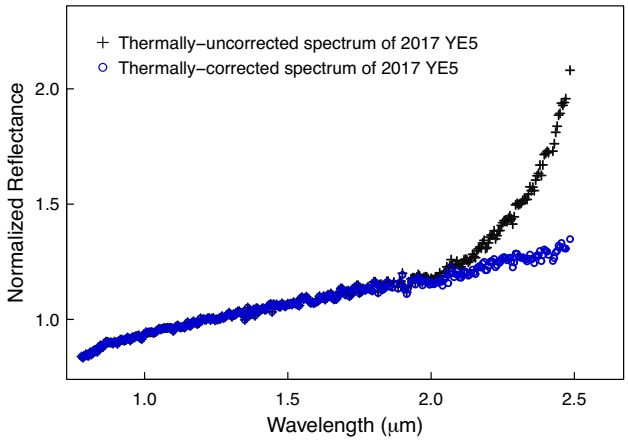

Figure 9. Near-IR spectrum of 2017 YE5 displaying a thermal emission at long wavelengths in the 2.5 μm range (black crosses) for which an albedo of 4 per cent was derived by fitting a thermal model. The blue circles depict the spectrum of the asteroid after removal of the modelled thermal excess. Both spectra have been normalized to unity at 1.25 μm. Taxonomic classification (D-type in this case) is derived from the thermally corrected spectrum.

spectrum for the object. A detailed description of the steps followed in the data reduction process can be found in Rivkin et al. (2004) and DeMeo & Binzel (2008). It is important to mention that the spectral data obtained by MITHNEOS has been continuously released for download and immediate use by the scientific community (e.g. Binzel et al. 2019).

3.2 Spectral characteristics of 2017 YE5

The spectrum of 2017 YE5 shows a distinct increase in reflectance in the near-IR wavelengths beyond 2 μm due to the presence of thermal emission (Fig. 9). Different studies have showed that, due to their relatively small distance from the Sun, low albedo NEAs usually show a thermal excess at the long wavelengths (Rivkin, Binzel & Bus 2005; Reddy et al. 2012). Thus, we were able to constrain the albedo value of 2017 YE5 using the methodology described in Rivkin et al. (2005) and references therein. This method includes the object's distances from Earth and Sun, the solar phase angle, slope parameter, albedo, emissivity (assumed to be 0.9), and the 'beaming' parameter (η).

Hence, to constrain the albedo of this object, we had to fit a thermal model to the measured thermal-infrared excess. This required estimating the reflectance without any thermal contribution emission in the 2.5 μm range. This was estimated by extrapolating a linear continuum from 1.5−1.8 μm to 2.5 μm. The measured thermal emission was fitted with a model thermal excess, using different beaming parameters (from 1 to 2), and allowing the albedo to be a fitted parameter. Then, this modelled thermal flux was subtracted from the measured thermal spectrum and the result is shown in Fig. 9. The best-fitting thermal model was found for an albedo of 0.04 and a thermal parameter $\eta = 1.25$. A reasonable fit was also found for an albedo of 0.02 and $\eta = 1.5$. The best-fitting albedo is determined as one that provides the lowest residual value between the thermally corrected spectrum and the extrapolation of the linear fit to the spectrum at wavelengths < 1.8 μm. This derived low-albedo confirms that 2017 YE5 is a possible dormant Jupiter-family comet.

Then, we used the thermally corrected spectrum to perform the taxonomic classification. It is important to mention that is very important to remove the thermal excess before carrying out the classification procedures. According to Binzel et al. (2019), the spectrum of the asteroid after the removal of the modeled thermal excess is then representative of the intrinsic reflectance properties of the surface material. In addition, in the Bus-DeMeo taxonomy the spectral slope is calculated and removed prior to calculating principal components (PC1', PC2', etc), i.e. before the taxonomy classification (DeMeo et al. 2009). This is useful to minimize reddening effects due to phase angle and space weathering that can influence the Bus-DeMeo classification.

The classification into the Bus-DeMeo system (DeMeo et al. 2009) was accomplished using the online taxonomy calculator (http://smass.mit.edu/busdemeoclass.html) developed by Stephen M. Slivan. Considering only the NIR spectrum, we classified 2017 YE5 as a D-type asteroid under this taxonomy system, with principal components $PC_{ir}1' = -0.1156$, $PC_{ir}2' = 0.1802$ and $PC_{ir}3' = 0.0340$. This spectrum shows a slope of 0.25, which is slightly larger than the minimum infrared slope for D-type asteroids (DeMeo et al. 2009). We also searched for the taxonomic classification using combined visible photometric and NIR spectra. This allowed us to note a very steep slope with a slight gentle curvature around 1.5 μm, which is commom in D-types. The 0.45–2.5 μm spectral range of 2017 YE5 shows a slope of 0.43, within the slope range of 0.38–1.5 identified for D-type asteroids (DeMeo et al. 2009), and principal components $PC1' = 0.1456$, $PC2' = -0.2402$ and $PC3' = -0.1407$. This classification is in good agreement with the determined low albedo of 2–4 per cent. Assuming an absolute magnitude of 19.2 provided by the JPL, the effective diameter of this object has a value between 0.96 and 1.36 km. This interval is consistent with the effective diameter of 1.27 km, which was calculated for the combined components each about 0.9 km, indicated by the radar observations (Taylor et al. 2019).

Regarding to the taxonomic classification, our result supports that 2017 YE5 has surface properties to be considered a dormant comet candidate. It is important to note that the spectrum of 2017 YE5 can have been affected by space weathering, whose effects on primitive asteroids are not yet clear. For example, reddening and bluing trends in the colours and spectra of primitive asteroids have been reported in the literature (e.g. Nesvorný et al. 2005; Lazzarin et al. 2006). This could explain the fact that the spectral slope and the principal components of 2017 YE5 are also similar to those expected for T-type asteroids (DeMeo et al. 2009).

4 DISCUSSION

Applying the Fourier analysis of the sum of two series to the light curves obtained at OASI and BMO, we found two additive light curves for the 2017 YE5 system. The best-fitting orbital period, $P_{orb} = 23.7$ h, was derived after removing the rotational light curve of $P_1 = 14.88$ h from the data using the dual-period search tool available in Canopus software. Our orbital period of about one day is in accordance with the value estimated by radar observations (Taylor et al. 2018, 2019). The primary period suggests that one of the components can be in a kind of spin–orbit resonance 5:8, indicating a possible asynchronous component or tumbling rotator in the system. The possibility of a non-principal axis rotator in this system, as well as a misaligned between the spin axes of the components were also suggested from the analysis of the radar data (Taylor et al. 2018, 2019). We also speculated on the possibility of a third more distant component in this system, but according to Patrick Taylor (private communication), nothing was found to suggest it in the radar images.

As seen with binaries like (69230) Hermes and (90) Antiope, systems with nearly equal-size components can tidally evolve to a

fully synchronous end state very rapidly, unlike systems with one large component and a second component much smaller (Taylor & Margot 2011). This occurs because the tidal time-scale is similar for each component of a high-mass ratio[2] system, which makes systems of this type evolve to a fully synchronized state faster (Jacobson & Scheeres 2011). The fact the 2017 YE5 system presents a possible asynchronous component indicates that the system is not fully synchronized, as expected for equal-size binaries, such as Hermes. Thus, we speculate that 2017 YE5 had a more recent formation than (69230) Hermes (Taylor & Margot 2011), since both binaries have similar sizes and semimajor axes, and probably their tidal synchronization time-scales as well. This could explain why 2017 YE5 has not yet reached a fully synchronized state. Another possible explanation could be that the components of this system have different compositions, which makes the syncronization process longer due to the difference between the masses of the components (Jacobson & Scheeres 2011). It is important to mention that almost all the nearly equal-mass binary asteroids are found in the main belt with the exception of the four members discovered in the NEA population, including the 2017 YE5. According to several studies, after these systems reach the doubly synchronous state, they will continue to evolve into contact binaries or asteroid pairs (McMahon & Scheeres 2010; Jacobson & Scheeres 2011; Scheirich et al. 2021).

A possible variation in surface composition was observed by comparing the two photometric spectra obtained in different photometric systems. We have shown that the two spectra have different behaviours with respect to the variation of reflectance as a function of wavelength. While the spectrum obtained with OAN-SPM data revealed a larger spectral slope than for D-type asteroids, the spectrum from OASI showed an attenuation in reflectance of about 0.8 μm that we do not see as an observational artefact, though we do not have the reflectance in z band in this last one. This finding means that the 2017 YE5 system could have components with compositional difference (different densities). This hypothesis is supported by radar observations that showed a distinct difference in the radar reflectivity of the two components (Taylor et al. 2018, 2019). Another possible explanation, however, could be that this object has undergone a change in the spectrum due to the presence of a dust coma in one of the components or another characteristic that could alter the behaviour of the spectrum, such as for example, different surface roughnesses probably produced by different erosive processes (e.g. thermal fracturing, micrometeoroid impacts, and volatile outgassing).

In addition, the colour indices determined from OAN-SPM data in the Johnson–Cousins system indicate that 2017 YE5 has a very reddish surface. We found $B - V = 0.682 \pm 0.276$, $V - R = 0.526 \pm 0.112$, $V - I = 1.073 \pm 0.113$, $B - R = 1.21 \pm 0.27$, and $R - I = 0.546 \pm 0.09$, which are colours very similar to those of various comets (and main belt comets), including the JFC 67P/Churyumov–Gerasimenko with $V - R = 0.52 \pm 0.05$ (Lamy et al. 2006) and the binary main belt comet 288P with $B - V = 0.67 \pm 0.04$, $V - R = 0.50 \pm 0.03$, and $B - R = 1.17 \pm 0.04$ (Agarwal et al. 2016). For comparison, our colour indices are almost identical to the mean value $V - R = 0.51 \pm 0.02$ obtained for the nuclei of 44 ecliptic comets and $V - R = 0.50 \pm 0.03$ considering only the nuclei of JFCs (Lamy & Toth 2009). The active JFCs have a mean $B - R = 1.22 \pm 0.02$, while the nuclei of JFCs have a slightly higher value ($B - R = 1.31 \pm 0.08$) (Jewitt 2015). D-types asteroids have a mean $B - R = 1.21 \pm 0.06$ and $V - I = 0.89 \pm 0.03$ (Ieva et al. 2018). Thus, the colours obtained in this work indicate that 2017 YE5 has a reddish surface than typical D-type asteroids (as shown in Fig. 6), which is consistent with several cometary nuclei, as shown in colour–colour diagram (Fig. 7). It is important to mention that D-type asteroids, considered primitive bodies,[3] have very low albedos and are expected to be rich in organic compounds, which could explain their strong red spectral slopes (Gradie & Veverka 1980; Emery et al. 2015)

We derived an average density for the 2017 YE5 system varying from 0.6 to 1.2 g cm^{-3}. It is worth mentioning that the density should increase slightly, assuming that the components are not spheres. This density interval is in good agreement with the reported densities for different D-type asteroids, including the binary Trojan asteroid (624) Hektor with 1.0 ± 0.02 g cm^{-3} (Marchis et al. 2014). It is also consistent with densities of comets and transneptunian objects (Carry 2012). The density range reported here also is in agreement with the value reported for the equal-size binary Trojan (617) Patroclus (P-type), whose density has been determined to be 0.88 ± 0.15 g cm^{-3} (Marchis et al. 2006). These low densities indicate a large internal macroporosity of order 50 per cent (Margot et al. 2015) and/or a significant low density material (i.e. ice) (Emery et al. 2015). Thus, very reddish objects (P- and D-types) and with low densities are thought to originate from the outer part of the Solar system (scattered disc) and afterwards implanted into the Trojans and the outer main-belt during the planetary migration (Morbidelli et al. 2005; Levison et al. 2009). In the case of 2017 YE5, a candidate binary comet ($T_J = 2.87$), its low density suggests that it was formed in a similar process to that of most small binary asteroids, that is, by rotational fission of a single progenitor with a rubble-pile structure.

Our near-infrared spectroscopic analysis confirmed that 2017 YE5 has a red featureless spectrum. We also noted that the photometric spectrum obtained with the OAN-SPM data is redder than the infrared spectrum. Both spectra were classified as a D-type in the Bus-DeMeo taxonomy, with the photometric spectrum showing a high slope of $S'_{vis} = 15 \pm 5$ per cent/1000 Å, and the infrared spectrum a slope of $S'_{ir} = 4 \pm 1$ per cent/1000 Å. The differences in the spectral slopes in the visible and near-infrared were analysed in Licandro et al. (2008, 2018) and are probably due to the typical curvature of D-type objects. Since the infrared spectrum of 2017 YE5 exhibits a thermal emission in about 2.5 μm, we were able to constrain its visible albedo to 2–4 per cent by applying a thermal model. This low albedo is within the typical values found for the comet nuclei, whose values vary from 2 to 6 per cent (Kim et al. 2014). For example, the JFC 67P has an albedo of 6 per cent (Bibring et al. 2015). Indeed, several studies have shown that the majority of NEAs in cometary orbits present featureless spectra (C-, P-, and D-types) and comet-like albedos (DeMeo & Binzel 2008; Licandro et al. 2008; Fernández & Sosa 2015; Licandro et al. 2018). In this regard, dynamical studies indicate that this sub-population of NEAs is composed of a significant fraction of objects come from JFCs (cometary origin) and from the outer main-belt (asteroidal origin) (e.g. Binzel et al. 2019). Therefore, it is possible that the 2017 YE5 system entered the NEAs space through one of these regions, with a greater probability for the first hyphotesis, as indicated by different studies (e.g. Fernández et al.

[2]Mass ratio is defined as the mass of the smaller component divided by the mass of the larger component of the binary system.

[3]Primitive asteroids are objects with visible geometric albedo less than 0.15 and featureless spectra in the visible. In the Tholen & Barucci (1989) taxonomy, which considers albedo and spectra, primitive asteroids are those the B-, C-, D-, F-, G-, P-, and T- types.

2005; DeMeo & Binzel 2008; Mommert et al. 2015; Licandro et al. 2018).

Primitive objects are most abundant in the outer region of the main belt and beyond. These objects are also present in the inner main belt and the NEA population, indicating that primitive NEAs were delivered from different regions, including a strong contribution from the Jupiter Family Comets (Binzel et al. 2019). D- and P-types asteroids are located mainly in the outer main belt and in the Jupiter Trojan population (Gil-Hutton & Licandro 2010; Emery et al. 2015). In particular, almost all the published spectra of comet nuclei are similar to the P- and D-types asteroids (Licandro et al. 2008). According to different studies, both asteroid classes are presumed to be similar to carbonaceous chondrites, but with a fraction of organic matter to explain the high spectral slopes (Gaffey, Bell & Cruikshank 1989; Vilas, Jarvis & Gaffey 1994; Cloutis et al. 2011; Fornasier, Clark & Dotto 2011). D-types, in particular, are probably similar to the reddest CI/CM chondrites and also to the Tagish Lake meteorite (an unusual carbonaceous chondrite), which is considered as the best meteorite analogue of this class (Fornasier et al. 2011; Herd et al. 2011; Cloutis et al. 2012). In this context, using the Modeling for Asteroids tool (M4AST; Popescu, Birlan & Nedelcu 2012), we have found that the combined spectrum of 2017 YE5 has a reasonable match with the Tagish Lake meteorite and, secondly, with CM2 carbonaceous meteorites, obtained from a least-squares search in the RELAB spectral data base. In both meteorites, it was found that water is incorporated into the phyllosilicate minerals (e.g. serpentine and saponite) formed by aqueous alteration (Cloutis et al. 2011; Fornasier et al. 2011). The Tagish Lake, in particular, contains an abundance of organic materials, nearly 3 weight percent (wt per cent), including amino acids (Herd et al. 2011). The density of CM meteorites varies from 1.79 to 2.40 g cm^{-3} (Britt & Consolmagno 2003), while that of Tagish Lake is of 1.5 g cm^{-3} (Brown et al. 2000). These values are higher than the estimated interval for 2017 YE5, indicating again that it has a large macroporosity and/or is composed of two components of different densities.

Knowing that 2017 YE5 is likely a dormant comet, we analysed their photometric profiles in search of a possible residual cometary activity, following the method described in Martino et al. (2019). Thus, the photometric profiles of 2017 YE5 were compared with profiles of field stars, in search of a widening of the asteroid profile that would indicate traces of cometary activity. It was possible to obtain four photometric profile of 2017 YE5 from OASI data, but with no clear signs of cometary activity in any of them, just a slight difference between the profiles of the stars and the object. Fig. 10 shows an example of the photometric profile of 2017 YE5 obtained from images taken on July 11th. In addition, photometric profiles may not be useful for identifying cometary activity in binary systems, since this method has only been used successfully for active single asteroids (Martino et al. 2019). We do not reject the possibility that the profile of 2017 YE5 has been affected by the presence of two components of almost equal size. We will investigate this possibility in an upcoming article, which will cover other almost equal-mass binary asteroids, including (90) Antiope, (809) Lundia, and (1139) Atami, for which we already have data obtained from OASI.

We also performed another analysis to investigate the possibility that the cometary activity may have occurred in the past. In this context, if 2017 YE5 was active in a certain period of time, is possible that it has left a trail of dusty debris in its path, which could eventually cross the Earth's orbit. Thus, we attempt to seek for parenthood between the binary 2017 YE5 and meteor activity. In this sense, we used video meteors data bases of Sonotaco, EDMOND and EXOSS (SonotaCo 2009; Rudawska et al. 2015; Jenniskens et al. 2016; Fernandes et al. 2020), in order to search for associations. Applying the methodology of Guennoun et al. (2019), we were able to compare many methods to obtain the most suitable one using a criterion threshold $D_{sh} < 0.2$ (Southworth & Hawkins 1963), considering 8° for the difference in Solar Longitude and a fixed threshold value for angular distance to the apparent radiant. This method also combines the radiant equatorial coordinates (α and δ) and geocentric velocity of the NEA (computed by Neslusan, Svoren & Porubcan (1998) program) and the meteoroids. Thus, we found a sample of 18 meteor orbits, originally classified as sporadics, that could be associated with 2017 YE5. A more detailed analysis using statistical test and numerical integration backward time of the orbit of the potential progenitors, modelling particles ejections, will be presented in an upcoming article, which will cover other NEAs in cometary orbits in order to explore past cometary activities through association with meteor showers.

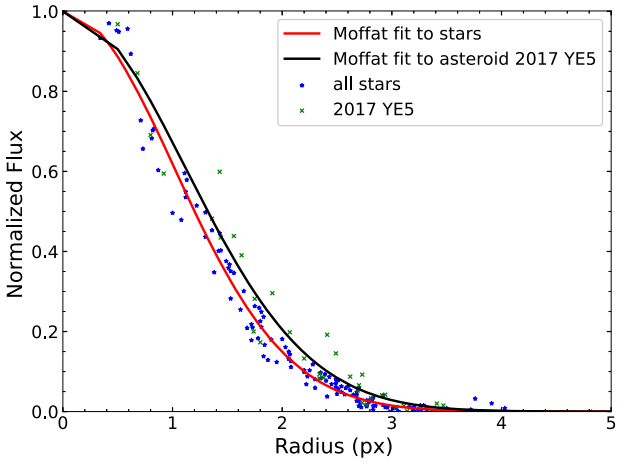

Figure 10. Photometric profile for the 2017 YE5 system. The plot contains the values of normalized flux as a function of the radius from the centroid (in pixels) for the stars (blue dots) and for the object (green dots), as well as the Moffat adjustment for the stars (red line) and for the object (black line).

It is interesting to note that many NEAs in cometary orbits, most of which are low-albedo objects, displayed at least one comet-like activity. Examples include NEA (3552) Don Quixote ($T_J = 2.31$), which was found to show cometary activity many years after its discovery as asteroid (Mommert et al. 2014), and NEA P/2006 HR30 ($T_J = 1.78$, Halley-type orbit), which was discovered as an asteroid and reclassified with the detection of coma (e.g. Hicks & Bauer 2007). (3552) Don Quixote is probably a dormant comet, since it is not clear if its activity is persistent or an outburst (Mommert et al. 2015). Also, some NEAs, such as (5496) 1973 NA ($T_J = 2.53$), 289P/Blanpain (2003 WY25) ($T_J = 2.82$) and 3552 Don Quixote, were associated with meteor showers (Williams & Collander-Brown 1998; Jewitt 2006; Rudawska & Vaubaillon 2015). Some typical NEAs also have shown cometary activity, such as NEA (4015) Wilson-Harrington ($T_J = 3.08$), which exhibited comet-like activity in 1949, but never since (e.g. Fernández et al. 1997), and NEA (3200) Phaethon ($T_J = 4.50$), which has been identified as the parent for the Geminid meteor shower (e.g. Jewitt, Hsieh & Agarwal 2015). Therefore, the study of comet-like NEAs is very important to understand the origin of terrestrial planet volatiles, since these objects probably played a fundamental role in the delivery of volatiles, water and organic materials to early Earth (e.g. Morbidelli et al. 2000; Izidoro et al. 2013).

In this context, primitive NEAs have and continue to be targeted by spacecraft missions. Recent examples include NEA (101955) Bennu, target of NASA's OSIRIS-REx (Lauretta et al. 2017), and (162173) Ryugu, target of JAXA's Hayabusa2 (Watanabe et al. 2017). In addition, various binary NEAs have been selected for different missions, including NEA (65803) Didymos, which is the target of the NASA's Double Asteroid Redirection Test (DART) mission (Naidu et al. 2020), NEAs (175706) 1996 FG3 and (35107) 1991 VH, which are the targets of the NASA's JANUS mission (Scheeres et al. 2021). Almost all these NEAs have been classified as primitive objects, except (35107) 1991 VH, a Sk-type, and Didymos, which was classified as Xk-type, and it is not clear if it is primitive. The active NEA (3200) Phaethon will be visited by JAXA's DESTINY+ mission, which is planned to be launched in 2024 (Arai et al. 2021). DART mission is a deflection experiment by kinetic impactor, while the others, in turn, have as their main focus the identification and understanding of the processes that lead to binary formation and evolution.

5 SUMMARY AND CONCLUSIONS

We observed the nearly equal-mass binary near-Earth asteroid 2017 YE5 after its close Earth flyby on 2018 June 21, when its binary nature was finally discovered. Our physical characterization of this system sheds light on its physical properties, including rotational and orbital period, albedo and taxonomic type, as well as its likely cometary origin. Based on our study we determined the following:

(i) We found that 2017 YE5 system has a mutual orbital period of $P_{\rm orb} = 23.706 \pm 0.006$ h and a primary rotational period of $P_1 = 14.88 \pm 0.01$ h, indicating a possible asynchronous component or non-principal axis rotator in this system. These results are in good agreement with those reported by radar observations.

(ii) We derived the mean density of 2017 YE5 is from 0.6 to 1.2 g cm^{-3}, implying a rubble-pile internal structure for the components. We do not reject the possibility of the low density to be due to combination of large macroporosity and volatiles compounds.

(iii) We obtained two photometric spectra (Figs 5 and 6), one using OAN-SPM data, which exhibits a high-spectral slope corresponding to a D-type, with spectral slope S' $= 15 \pm 5$ per cent/1000 Å, and another using OASI data, which shows a different behaviour, such as a Q-type. This difference suggests that the components of the 2017 YE5 system can have different compositions. The OASI spectrum showed an attenuation of the reflectance in the *i* band (*SDSS* filter), which is not well understood due to the lack of the reflectance in the *z* band.

(iv) We found that the colour indices determined for 2017 YE5 from OAN-SPM data indicate a very red surface, consistent with the D-type asteroids and JFC nuclei. The colors found were $B - V = 0.682 \pm 0.276$, $V - R = 0.526 \pm 0.112$, $V - I = 1.073 \pm 0.113$, $B - R = 1.21 \pm 0.27$, and $R - I = 0.546 \pm 0.09$.

(v) We applied a thermal model fit to the infrared spectrum, yielding a dark albedo of 2−4 per cent, with a best fit $\eta = 1.25$. An effective diameter was estimated to be 0.96–1.36 km (assuming $H = 19.2$).

(vi) We classified the thermally corrected spectrum as a D-type in the Bus-DeMeo taxonomy and, using combined visible photometric and NIR spectra, we also found a reasonable match with D-type asteroids. This classification is very consistent with the best-fit albedo.

(vii) From the comparison with laboratory spectra (RELAB data base), we found that 2017 YE5 has a reasonable match with the Tagish Lake meteorite. Therefore, it is very likely that 2017 YE5 to contain water incorporated into phyllosilicate minerals (e.g. serpentine) formed by aqueous alteration. Also, it is possible that there is a significant fraction of organic materials and volatiles compounds in its composition.

(viii) We suggest that 2017 YE5 has a cometary origin, due to its comet-like albedo and orbit ($T_{\rm J} = 2.87$). It is important to mention that, while suggesting that 2017 YE5 is a dormant Jupiter-family binary comet, we do not reject that it came from the outer main-belt.

We were able to constrain some physical properties of the 2017 YE5 and compare them with those previously reported from radar observations. Only four nearly equal-size binary NEA have been reported in the literature, including this work, and only 2017 YE5 has been classified as D-type asteroid to date. In addition, 2017 YE5 is the first binary NEA discovered in a typical Jupiter-family comet orbit. Further observations of this object are needed to confirm the composition of the two components and to improve our understanding about its rotation state. The next favourable viewing geometry will only occur in 2037 February with $V \approx 19.5$, when it will pass at a nominal distance of approximately 0.238 au from Earth. Given its comet-like albedo and orbit, the next opportunities for additional observations with large telescopes may provide further clues to the origin and formation of this rare binary NEA.

ACKNOWLEDGEMENTS

F.M. thanks the Foundation for Research Support of the State of Rio de Janeiro (FAPERJ) for the financial support (E-26/201.877/2020). E.R., M.S., M.C. and P.A. acknowledge the diverse fellowships granted by Coordination for the Improvement of Higher Education Personnel (CAPES) and National Council for Scientific and Technological Development (CNPq). D.L. thanks for research support given by CNPq (305409/2016-6) and FAPERJ (E-26/202.841/2017). L.S. thanks the fellowship granted by Research Support Foundation of the State of São Paulo (FAPESP) (2016/18418-0). The authors are grateful to the IMPACTON team and, in particular, to R. Souza and A. Santiago for the technical support, and the OAN-SPM team. The authors are also grateful to Andy Rivkin for help with the correction of spectrum for thermal excess in order to constrain the albedo. Finally, the authors thanks the referee Gonzalo Tancredi for useful comments that helped improve this paper.

The Infrared data utilized in this publication were obtained and made available by the MITHNEOS MIT-Hawaii Near-Earth Object Spectroscopic Survey. The IRTF is operated by the University of Hawaii under contract 80HQTR19D0030 with the National Aeronautics and Space Administration (NASA). The MIT component of this work is supported by NASA grant 80NSSC18K0849.

Taxonomic type result presented in this work was determined using a Bus-DeMeo Taxonomy Classification Web tool by Stephen M. Slivan, developed at MIT with the support of National Science Foundation Grant 0506716 and NASA Grant NAG5-12355.

This article is based on observations obtained at the Observatório Astronômico do Sertão de Itaparica (OASI, Itacuruba) of the Observatório Nacional, Brazil, and at the Blue Mountains Observatory (Australia), and at the Observatorio Astronómico Nacional de San Pedro Mártir (OAN-SPM) operated by the Universidad Nacional Autónoma de México (UNAM). The research work at Blue Mountains Observatory is supported and promoted by the 2015 Shoemaker NEO Grant.

DATA AVAILABILITY

The data underlying this study are available in the article.

REFERENCES

Agarwal J., Jewitt D., Weaver H., Mutchler M., Larson S., 2016, AJ, 151, 12
Arai T. et al., 2021, Lunar and Planetary Science Conference. Lunar and Planetary Science Conference. p. 1896
Bibring J. P. et al., 2015, Science, 349, 493
Binzel R. P. et al., 2019, Icarus, 324, 41
Britt D. T., Consolmagno G. J., 2003, Meteorit. Planet. Sci., 38, 1161
Brown P. G. et al., 2000, Science, 290, 320
Carry B., 2012, Planet. Space Sci., 73, 98
Carvano J. M., Davalos J. A. G., 2015, A&A, 580, A98
Carvano J. M., Hasselmann P. H., Lazzaro D., Mothé-Diniz T., 2010, A&A, 510, A43
Cloutis E. A., Hudon P., Hiroi T., Gaffey M. J., Mann P., 2011, Icarus, 216, 309
Cloutis E. A., Hudon P., Hiroi T., Gaffey M. J., Mann P., 2012, Icarus, 221, 984
DeMeo F., Binzel R. P., 2008, Icarus, 194, 436
DeMeo F. E., Binzel R. P., Slivan S. M., Bus S. J., 2009, Icarus, 202, 160
Emery J. P., Marzari F., Morbidelli A., French L. M., Grav T., 2015, Asteroids IV. p. 203–220
Fernández J. A., Sosa A., 2015, Planet. Space Sci., 118, 14
Fernández Y. R., McFadden L. A., Lisse C. M., Helin E. F., Chamberlin A. B., 1997, Icarus, 128, 114
Fernández Y. R., Jewitt D. C., Sheppard S. S., 2005, AJ, 130, 308
Fernandes F. C. R., Carita L. A., Rodrigues I., Pimentel G. J. A., Silva R. C. A., Matos P. B., Reis de Castro V. D., Oliveira J. C., 2020, J. Int. Meteor. Organ., 48, 173
Fornasier S., Clark B. E., Dotto E., 2011, Icarus, 214, 131
Gaffey M. J., Bell J. F., Cruikshank D. P., 1989, in Binzel R. P., Gehrels T., Matthews M. S., eds, Asteroids II. p. 98
Gil-Hutton R., Licandro J., 2010, Icarus, 206, 729
Gradie J., Veverka J., 1980, Nature, 283, 840
Guennoun M., Vaubaillon J., Čapek D., Koten P., Benkhaldoun Z., 2019, A&A, 622, A84
Hanuš J. et al., 2011, A&A, 530, A134
Hanuš J. et al., 2013, A&A, 551, A67
Hapke B., 1981, J. Geophys. Res., 86, 3039
Hapke B., 1984, Icarus, 59, 41
Hapke B., 2001, J. Geophys. Res., 106, 10039
Harris A. W. et al., 1989, Icarus, 77, 171
Herd C. D. K. et al., 2011, Science, 332, 1304
Hicks M. D., Bauer J. M., 2007, ApJ, 662, L47
Ieva S. et al., 2018, A&A, 615, A127
Izidoro A., de Souza Torres K., Winter O. C., Haghighipour N., 2013, ApJ, 767, 54
Jacobson S. A., Scheeres D. J., 2011, Icarus, 214, 161
Jenniskens P. et al., 2016, Icarus, 266, 384
Jester S. et al., 2005, AJ, 130, 873
Jewitt D., 2006, AJ, 131, 2327
Jewitt D., 2015, AJ, 150, 201
Jewitt D., Hsieh H., Agarwal J., 2015, Asteroids IV. p. 221
Kim Y., Ishiguro M., Usui F., 2014, ApJ, 789, 151
Lamy P., Toth I., 2009, Icarus, 201, 674
Lamy P. L., Toth I., Weaver H. A., Jorda L., Kaasalainen M., Gutiérrez P. J., 2006, A&A, 458, 669
Landolt A. U., 1992, AJ, 104, 340
Lauretta D. S. et al., 2017, Space Sci. Rev., 212, 925
Lazzarin M., Marchi S., Moroz L. V., Brunetto R., Magrin S., Paolicchi P., Strazzulla G., 2006, ApJ, 647, L179
Lazzaro D., Barucci M. A., Perna D., Jasmim F. L., Yoshikawa M., Carvano J. M. F., 2013, A&A, 549, L2
Levison H. F., Duncan M. J., 1994, Icarus, 108, 18
Levison H. F., Bottke W. F., Gounelle M., Morbidelli A., Nesvorný D., Tsiganis K., 2009, Nature, 460, 364
Licandro J., Alvarez-Candal A., de León J., Pinilla-Alonso N., Lazzaro D., Campins H., 2008, A&A, 481, 861
Licandro J., Popescu M., de León J., Morate D., Vaduvescu O., De Prá M., Ali-Laoga V., 2018, A&A, 618, A170
Luu J. X., Jewitt D. C., 1996, AJ, 111, 499
Marchis F. et al., 2006, Nature, 439, 565
Marchis F. et al., 2014, ApJ, 783, L37
Margot J. L., Nolan M. C., Benner L. A. M., Ostro S. J., Jurgens R. F., Giorgini J. D., Slade M. A., Campbell D. B., 2002, Science, 296, 1445
Margot J.-L., Pravec P., Taylor P., Carry B., Jacobson S., 2015, in Michel P., DeMeo F. E., Bottke W. F., eds, Asteroids IV. p. 355
Martino S., Tancredi G., Monteiro F., Lazzaro D., Rodrigues T., 2019, Planet. Space Sci., 166, 135
McMahon J., Scheeres D., 2010, Icarus, 209, 494
Merline W. J., Weidenschilling S. J., Durda D. D., Margot J. L., Pravec P., Storrs A. D., 2002, Asteroids II. p. 289
Mommert M. et al., 2014, ApJ, 781, 25
Mommert M. et al., 2015, AJ, 150, 106
Morbidelli A., Chambers J., Lunine J. I., Petit J. M., Robert F., Valsecchi G. B., Cyr K. E., 2000, Meteorit. Planet. Sci., 35, 1309
Morbidelli A., Levison H. F., Tsiganis K., Gomes R., 2005, Nature, 435, 462
Mothé-Diniz T., Lazzaro D., Carvano J. M., Florczak M., 2000, Icarus, 148, 494
Murchie S. L., Pieters C. M., 1996, J. Geophys. Res., 101, 2201
Naidu S. P. et al., 2020, Icarus, 348, 113777
Neslusan L., Svoren J., Porubcan V., 1998, A&A, 331, 411
Nesvorný D., Jedicke R., Whiteley R. J., Ivezić Ž. 2005, Icarus, 173, 132
Pieters C. M., Noble S. K., 2016, J. Geophys. Res. (Planets), 121, 1865
Popescu M., Birlan M., Nedelcu D. A., 2012, A&A, 544, A130
Pravec P., Harris A. W., 2007, Icarus, 190, 250
Pravec P. et al., 2005, Icarus, 173, 108
Pravec P. et al., 2006, Icarus, 181, 63
Pravec P. et al., 2010, Nature, 466, 1085
Ramírez I. et al., 2012, ApJ, 752, 5
Rayner J. T., Toomey D. W., Onaka P. M., Denault A. J., Stahlberger W. E., Vacca W. D., Cushing M. C., Wang S., 2003, PASP, 115, 362
Reddy V., Gaffey M. J., Abell P. A., Hardersen P. S., 2012, Icarus, 219, 382
Rivkin A. S., Binzel R. P., Sunshine J., Bus S. J., Burbine T. H., Saxena A., 2004, Icarus, 172, 408
Rivkin A. S., Binzel R. P., Bus S. J., 2005, Icarus, 175, 175
Rondón E., Arcoverde P., Monteiro F., Medeiros H., Navas G., Lazzaro D., Carvano J. M., Rodrigues T., 2019, MNRAS, 484, 2499
Rondón E. et al., 2020, PASP, 132, 065001
Rondón-Briceño E., Carvano J. M., Lorenz-Martins S., 2017, MNRAS, 468, 1556
Rubincam D. P., 2000, Icarus, 148, 2
Rudawska R., Vaubaillon J., 2015, Planet. Space Sci., 118, 25
Rudawska R., Matlovič P., Tóth J., Kornoš L., 2015, Planet. Space Sci., 118, 38
Sanchez J. A., Reddy V., Nathues A., Cloutis E. A., Mann P., Hiesinger H., 2012, Icarus, 220, 36
Scheeres D. J. et al., 2021, Lunar and Planetary Science Conference.. p. 1706
Scheirich P., Pravec P., 2009, Icarus, 200, 531
Scheirich P. et al., 2021, Icarus, 360, 114321
Smith J. A. et al., 2002, AJ, 123, 2121
Solontoi M. et al., 2012, Icarus, 218, 571
SonotaCo, 2009, J. Int. Meteor Organ., 37, 55
Southworth R. B., Hawkins G. S., 1963, Smithsonian Contributions to Astrophysics, 7, 261
Strazzulla G., Dotto E., Binzel R., Brunetto R., Barucci M. A., Blanco A., Orofino V., 2005, Icarus, 174, 31
Taylor P. A., Margot J.-L., 2011, Icarus, 212, 661

Taylor P. A. et al., 2018, AAS/Division for Planetary Sciences Meeting Abstracts. p. 50 508.07
Taylor P. A. et al., 2019, Lunar and Planetary Science Conference. p. 2945
Tholen D. J., Barucci M. A., 1989, in Binzel R. P., Gehrels T., Matthews M. S., eds, Asteroids II. p. 298
Vilas F., Jarvis K. S., Gaffey M. J., 1994, Icarus, 109, 274
Vokrouhlický D., Nesvorný D., Bottke W. F., 2003, Nature, 425, 147
Walsh K. J., Jacobson S. A., 2015, Asteroids IV. p. 375
Walsh K. J., Richardson D. C., Michel P., 2008, Nature, 454, 188
Warner B. D., 2018, Minor Planet Bull., 45, 366
Watanabe S.-i., Tsuda Y., Yoshikawa M., Tanaka S., Saiki T., Nakazawa S., 2017, Space Sci. Rev., 208, 3
Williams I. P., Collander-Brown S. J., 1998, MNRAS, 294, 127
Zellner B., Tholen D. J., Tedesco E. F., 1985, Icarus, 61, 355

This paper has been typeset from a TEX/LATEX file prepared by the author.